Tiedemann, R., Mix, A.C., Richter, C., and Ruddiman, W.F. (Eds.)
Proceedings of the Ocean Drilling Program, Scientific Results Volume 202

13. Pliocene Mixed-Layer Oceanography for Site 1241, Using Combined Mg/Ca and $\delta^{18}O$ Analyses of *Globigerinoides sacculifer*[1]

Jeroen Groeneveld,[2,4] Silke Steph,[2,5] Ralf Tiedemann,[2,5]
Dieter Garbe-Schönberg,[3] Dirk Nürnberg,[2] and Arne Sturm[2,5]

ABSTRACT

To reconstruct changes in tropical Pacific surface hydrography, we used samples from Site 1241 (5°50′N, 86°26′W; 2027-m water depth) to establish high-resolution records of Mg/Ca and $\delta^{18}O$ for the mixed-layer dwelling planktonic foraminifer *Globigerinoides sacculifer* for the Pliocene time interval from 4.8 to 2.4 Ma. An increase in average sea-surface temperatures (SSTs) (24.5°–25.5°C) between 4.8 and 3.7 Ma can probably be explained by a southward shift of the Intertropical Convergence Zone, thereby increasing the influence of the warmer North Equatorial Countercurrent.

The general global cooling trend, a response to intensification of Northern Hemisphere glaciation (NHG), started at ~3.2 Ma (shown by the $\delta^{18}O_{benthic}$ record) and is paralleled by tropical east Pacific cooling (indicated by $SST_{Mg/Ca}$). Tropical east Pacific cooling, however, had already commenced by ~3.7 Ma, suggesting that global cooling, probably related to decreasing atmospheric CO_2 concentrations, might have started well before intensification of NHG.

Relative changes in local sea-surface salinity (indicated by $\delta^{18}O_{salinity}$) show a decoupling from global high-latitude processes (shown by the $\delta^{18}O_{benthic}$ record). Long-term regional freshening started with decreasing $SST_{Mg/Ca}$ at ~3.7 Ma, suggesting that changes in the tropical wind field combined with latitudinal shifts of the tropical rainbelt were re-

[1] Groeneveld, J., Steph, S., Tiedemann, R., Garbe-Schönberg, D., Nürnberg, D., and Sturm, A., 2006. Pliocene mixed-layer oceanography for Site 1241, using combined Mg/Ca and $\delta^{18}O$ analyses of *Globigerinoides sacculifer*. *In* Tiedemann, R., Mix, A.C., Richter, C., and Ruddiman, W.F. (Eds.), *Proc. ODP, Sci. Results,* 202: College Station, TX (Ocean Drilling Program), 1–27. doi:10.2973/odp.proc.sr.202.209.2006
[2] Leibniz-Institute of Marine Sciences, IFM-GEOMAR, Wischhofstrasse 1-3, 24148 Kiel, Germany.
[3] Institute of Geosciences, University of Kiel, Germany.
[4] Present address: Research Center of Ocean Margins, Bremen University, Bremen, Germany.
jgroeneveld@uni-bremen.de
[5] Present address: Alfred Wegener Institute for Polar and Marine Research, Columbusstrasse, 27568 Bremerhaven, Germany.

Initial receipt: 15 November 2004
Acceptance: 10 August 2006
Web publication: 8 November 2006
Ms 202SR-209

lated to general decreases in tropical east Pacific SST-controlled $\delta^{18}O_{salinity}$.

The similarity of Pliocene $SST_{Mg/Ca}$ for *G. sacculifer* with modern SSTs in the east Pacific, in combination with the early development of a shallow thermocline at Site 1241, gives no direct support to the idea that a permanent El Niño-like Pliocene climate might have existed during the early Pliocene.

INTRODUCTION

We present combined high-resolution planktonic Mg/Ca and $\delta^{18}O$ records from tropical east Pacific Site 1241 that span the interval from 4.8 to 2.4 Ma. Site 1241 (5°50′N, 86°26′W) is situated at a water depth of 2027 m on the northern side of Cocos Ridge in the Guatemala Basin (Fig. F1). We combined the Mg/Ca and $\delta^{18}O$ records to determine $\delta^{18}O_{water}$. By subtracting an estimate of the Pliocene ice volume signal from the $\delta^{18}O_{water}$ record, we reconstructed a $\delta^{18}O_{salinity}$ record, which is assumed to represent relative changes in local sea-surface salinity (SSS). These results provide important information on Pliocene climate variability and shed light on the hypothesis of a permanent El Niño-like Pliocene climate and intensification of Northern Hemisphere glaciation (NHG).

The Pliocene was affected by two major global events: intensification of NHG and closure of the Panamanian Gateway. Both processes led to marked changes in global oceanography and climate (Maier-Reimer et al., 1990; Tiedemann and Franz, 1997; Billups et al., 1999; Haug et al., 2001). The Pliocene time interval prior to NHG is often used as a possible near-future analog because at that time, average temperatures were significantly warmer than today with atmospheric CO_2 concentrations probably slightly higher than modern ones (Dowsett et al., 1996; Crowley, 1996; Raymo et al., 1996). If Pliocene atmospheric CO_2 concentrations were higher than today, one could also expect higher tropical sea-surface temperatures (SSTs). More recently, modeling studies suggest the warm Pliocene represents a permanent El Niño-like state with a suppressed temperature difference between the western Pacific warm pool (WPWP) and the eastern Pacific cold tongue (Molnar and Cane, 2002, Fedorov et al., 2006), which is supported by Pliocene $\delta^{18}O_{G.sacculifer}$ gradients between the east and west Pacific (Cannariato and Ravelo, 1997; Chaisson and Ravelo, 2000; Ravelo et al., 2006).

TROPICAL PACIFIC OCEANOGRAPHY

The present-day location of Site 1241 (5°50′N, 86°26′W) is within the eastward-flowing North Equatorial Countercurrent (NECC). A tectonic backtrack of the Cocos plate, on which Site 1241 is positioned, locates Site 1241 at a more southwesterly position around 3°N, 87.7°W between 4 and 5 Ma (Mix, Tiedemann, Blum, et al., 2003; Pisias et al., 1995) (Fig. F1). The closer proximity to the equatorial divergence and the South Equatorial Current (SEC) suggests that expected SST and SSS at Site 1241 for the early Pliocene were ~0.5°–1°C cooler and 0.35 units less saline than present, if other physical properties remained unchanged (Mix, Tiedemann, Blum, et al., 2003). Surface hydrography in the tropical Pacific is strongly controlled by seasonal variations in wind

F1. Present-day SST and SSS distribution, p. 20.

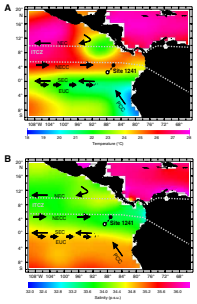

strength, causing seasonal changes in thermocline depth. In general, the NECC is closely linked to the Intertropical Convergence Zone (ITCZ), the zone of maximum heating and convergence of the northeast and southeast trade winds (Donguy and Meyers, 1996; Huber, 2002). North of the ITCZ, the northeast trade winds drive the North Equatorial Current toward the west and the southeast trade winds drive the SEC also to the west, but south of the ITCZ. Below the SEC and the equator, the Equatorial Undercurrent (EUC) flows toward the east from a depth of ~300 m in the WPWP to a depth of ~30 m in the east Pacific, parallel to the shallowing thermocline. The EUC is driven by the west-east pressure gradient and confined by the Coriolis force to the equator between 2°N and 2°S (Fig. **F1**). From August to December, the ITCZ is in its northernmost position and the southeast trade winds are at maximum strength, resulting in a strong SEC and NECC. The SEC carries cool waters from the southeastern upwelling areas to the west, and the NECC carries warm, low-salinity waters to the east out of the WPWP, depressing the thermocline (Donguy and Meyers, 1996). During this interval, the EUC is very weak. From March to May the ITCZ is at its southernmost position and the southeast trade winds are weak. As a result, the SEC and NECC are also weak. The EUC, in contrast, strengthens and causes the thermocline to shoal (Halpern and Weisberg, 1989; Ravelo and Shackleton, 1995). During El Niño events, easterly winds in the tropical Pacific become very weak, warm waters from the WPWP flow to the east, the thermocline deepens, the EUC is very weak, and SST increases, resulting in a decreased west-east SST gradient (Wallace et al., 1998).

Between the Atlantic/Caribbean and the east Pacific, a salinity gradient of 1–1.5 units exists, which is mainly determined by the net transport of water vapor from the Caribbean Sea over Central America into the east Pacific by the trade winds (Weyl, 1968; Zaucker et al., 1994). During the early Pliocene, free exchange of surface watermasses between the east Pacific and the Caribbean was still possible because of the open Panamanian Gateway. A salinity gradient did not develop because the inflow of lower salinity waters from the Pacific into the Caribbean prevented a significant salinity increase in the Caribbean. Haug et al. (2001) and Keigwin (1982) showed that $\delta^{18}O_{G.sacculifer}$ records of the east Pacific and the Caribbean started to diverge between 4.7 and 4.2 Ma. This was interpreted as an indication that the Isthmus of Panama had shoaled to a depth of <100 m, thereby restricting the inflow of low-salinity Pacific surface water masses into the Caribbean.

Notably, the present-day east Pacific is characterized by relatively low temperatures. The southeast trade winds cause strong upwelling along the Peruvian coast and along the equator, thus forming the Pacific cold tongue, which extends toward the west along the equatorial divergence (Mitchell and Wallace, 1992). Accordingly, the thermocline in these areas is very shallow (<50 m). In contrast, the Caribbean/western Atlantic warm pool is marked by a distinctly deeper thermocline (100–150 m). At a water depth of 50 m, the temperature contrast between the Caribbean and the east Pacific is 5°–6°C, whereas at the surface, SST is ~27°C, both at Site 1241 and in the Caribbean (Levitus and Boyer, 1994). North of the equator, however, SSTs rise and form the eastern Pacific warm pool (EPWP), which is characterized by seasonally maximum SSTs over 28.5°C and extends between 7°N and 27°N and as far west as 110°W (Wang and Enfield, 2001; Xie et al., 2005). An important feature of the EPWP is upwelling in the Costa Rica Dome (centered at 9°N, 90°W), a permanent cyclonic eddy possibly caused by strong "gap winds" blow-

ing through the Papagayo gap in the Central American cordillera (Umatani and Yamagata, 1991; Xie et al., 2005).

Molnar and Cane (2002) described the early Pliocene as a period of permanent El Niño-like conditions. During a present-day El Niño, the collapse of the easterlies leads to an equatorial Kelvin wave, which is characterized by the eastward flow of warm waters from the WPWP toward the east Pacific. This causes the cessation of upwelling, a decreasing temperature gradient between the WPWP and the east Pacific, and deepening of the thermocline in the east Pacific (Wallace et al., 1998). A permanent El Niño-like climate state during the Pliocene should thus be characterized by significantly higher $SST_{Mg/Ca}$ in the mixed layer than is found in present-day SSTs in the east Pacific, or by lower SSTs in the WPWP. The presence of a deeper thermocline can be confirmed by using the $\delta^{18}O$ and Mg/Ca records of planktonic foraminifers living at different water depths and calculating their gradients (**Steph et al.,** this volume).

MG/CA PALEOTHERMOMETRY

Mg/Ca is an independent paleotemperature proxy that is measured on the same biotic carrier as $\delta^{18}O$, which allows reconstruction of $\delta^{18}O_{water}$ and salinity variations without the problems introduced by other temperature proxies like different seasonal signals or different habitat depths of the biotic carriers (Nürnberg, 2000; Lea et al., 2002; Schmidt et al., 2004). Although Mg/Ca paleothermometry is well established for the last glacial–interglacial cycles, few $SST_{Mg/Ca}$ high-resolution records yet exist for older time periods (Tripati et al., 2003; Shevenell et al., 2004; Ravelo et al., 2006). Here, we present a high-resolution (<5 k.y./sample) Mg/Ca record for the early Pliocene, covering 2.4 m.y.

The application of Mg/Ca paleothermometry to Pliocene sample material demands consideration of possible changes in $Mg/Ca_{seawater}$. Brown (1996) showed in a cultivating experiment that a linear dependence between $Mg/Ca_{solution}$ and Mg/Ca_{foram} exists (0.1 mol/mol change in $Mg/Ca_{seawater}$ leads to 0.059 mmol/mol change in Mg/Ca_{foram}). Recently, Ries (2004) showed that several carbonate-building organisms display an exponential relationship between $Mg/Ca_{organism}$ and $Mg/Ca_{solution}$. The residence time of Mg in seawater is ~13 m.y. (Broecker and Peng, 1982), which suggests that paleo-SST reconstructions on shorter timescales would not be affected by a change in $Mg/Ca_{seawater}$. However, concentrations of Mg and Ca in seawater may be affected by several factors, including varying continental weathering rates (Berner et al., 1983; Wilkinson and Algeo, 1989), hydrothermal alteration of basalt at mid-ocean ridges (Mottl and Wheat, 1994; Elderfield and Schultz, 1996), carbonate deposition (Wilkinson and Algeo, 1989), and ion exchange reactions of Mg with clays (Gieskes and Lawrence, 1981). Several models that have attempted to reconstruct the Mg/Ca ratio of Cenozoic seawater suggest lower $Mg/Ca_{seawater}$ values than today (Wilkinson and Algeo, 1989; Stanley and Hardie, 1998).

Based on the models of Wilkinson and Algeo (1989) and Stanley and Hardie (1998), we assume a maximum lowering of 0.4 mol/mol in $Mg/Ca_{seawater}$ for the Pliocene time interval from 4.8 to 2.4 Ma. Applying the relationship of Brown (1996) between $Mg/Ca_{seawater}$ and Mg/Ca_{foram}, this implies a maximum underestimation of our SSTs by 0.7°–1.0°C. Because

this constant offset is within the error estimation for the SST reconstruction, we consider the Pliocene reduction in $Mg/Ca_{seawater}$ to be of minor importance.

METHODS

The Mg/Ca analyses for Site 1241 (5°50′N, 86°26′W) were performed on the planktonic foraminifer *Globigerinoides sacculifer. G. sacculifer* has a supposed habitat depth within the mixed layer of 30–50 m (Fairbanks et al., 1982; Curry et al., 1983). For each sample, 20–25 specimens from the 355- to 400-µm fraction were picked. Specimens with a saclike final chamber or visibly contaminated specimens were not selected for analysis. In case of insufficient numbers of specimens, the 250- to 355-µm fraction was used to provide additional material, from which as many as 35 specimens were picked. The bias introduced by extending the size fraction amounts to <0.5°C (Elderfield et al., 2002). The shallow water depth (2028 m) of the core in comparison with the depth of the east Pacific lysocline (3600 m) (Lyle et al., 1995) indicates that no significant dissolution has occurred. Fe/Ca and Mn/Ca analyses were performed to monitor contamination by clays or Mn carbonates and showed that the samples were not contaminated.

After gentle crushing, the samples were cleaned according to the cleaning protocol of Barker et al. (2003). To remove clays, the samples were rinsed 4–6 times with distilled deionized water and twice with methanol (suprapur) with an ultrasonic cleaning step (2–3 min) after each rinse. Samples from several intervals were subject to severe fragmentation during ultrasonic treatment. Therefore, the duration of ultrasonic treatment was reduced to a maximum of 1 min per treatment for these samples. Subsequently, samples were treated with a hot (97°C) oxidizing 1% $NaOH/H_2O_2$ solution (10 mL 0.1-N NaOH [analytical grade] + 100 µL 30% H_2O_2 [suprapur]) for 10 min to remove organic matter. Every 2.5 min the vials were rapped on the bench-top to release any gaseous build-up. After 5 min, the samples were placed in an ultrasonic bath for a few seconds in order to maintain contact between reagent and sample. This treatment was repeated after refreshing the oxidizing solution. Any remaining oxidizing solution was removed by three rinsing steps with distilled deionized water. After transferring the samples into clean vials, a weak acid leach with 250 µL of 0.001-M HNO_3 (subboiled distilled) was applied with 30-s ultrasonic treatment and two subsequent rinses with distilled deionized water. After cleaning, the samples were dissolved in 0.075-M nitric acid (HNO_3) (subboiled distilled) and diluted several times so that all samples were expected to have Ca concentrations in the range 30–70 ppm, the ideal range for analysis (Garbe-Schönberg et al., unpubl. data).

Analyses were performed on a simultaneous, radially viewing inductively coupled plasma–optical emission spectrometer (Ciros CCD SOP, Spectro A.I., Germany) at the Institute of Geosciences (Kiel University, Kiel, Germany). A cooled cyclonic spray chamber in combination with a microconcentric nebulizer (200 µL/min sample uptake) was optimized for best analytical precision and minimized uptake of sample solution. Automated sample introduction was via an autosampler (Spectro A.I.). For Ca, we used the spectral line with the highest stability (183.801 nm), providing a truly simultaneous analysis with Mg and Sr within the same detector read-out phase. For Mg and Sr, we used the emission lines with the highest signal-to-noise ratios (279.553 nm for Mg and 407.771

nm for Sr). For Fe and Mn, we used the emission lines with the highest sensitivity (259.940 nm for Fe and 257.610 nm for Mn). Matrix effects caused by varying concentrations of Ca were cautiously checked and were found not to be significant (Garbe-Schönberg et al., unpubl. data).

Analytical sessions with batches of 200–300 samples usually took between 20 and 30 hr, during which the drift of the instrument could be neglected, being <0.2% as determined by analyzing an internal consistency standard after every five samples. The analytical error for analysis of Mg/Ca ratios was 0.1% for a total of 600 samples. Replicate analyses on the same samples, which were cleaned and analyzed during different sessions, showed a standard deviation of 0.09 mmol/mol, introducing a temperature error of ~0.5°C. The conversion of foraminiferal Mg/Ca ratios into SSTs was carried out by applying the equation of Nürnberg et al. (2000):

$$SST = [\log (Mg/Ca) - \log 0.491]/0.033.$$

For stable isotope analysis, 10 specimens of *G. sacculifer* (without sac-like final chamber) were picked from the 355- to 400-µm fraction. All isotope analyses were run at IFM-GEOMAR (Kiel, Germany) on a Finnigan Delta-Plus Advantage mass spectrometer coupled to a Finnigan/Gas Bench II. Analytical external precision was better than 0.07‰ for $\delta^{18}O$ (±1σ). The values are reported relative to Peedee belemnite, based on calibrations directly to National Bureau of Standards 19.

The age model for Site 1241 was constructed by matching cyclic variation patterns in climate proxy records of $\delta^{18}O_{benthic}$, $\delta^{13}C_{benthic}$, and percent sand with patterns of changes in solar radiation that are controlled by cyclic variations in Earth's orbital parameters. This astronomically derived age model is in agreement with the most recent astronomical polarity timescale and with other orbitally tuned age models. The establishment of the age model is described in detail in **Tiedemann et al.** (this volume).

RESULTS

Mg/Ca ratios of *G. sacculifer* vary between 2.50 and 3.88 mmol/mol for the studied time interval (4.8–2.4 Ma) (Fig. **F2A**), providing $SST_{Mg/Ca}$ of 21.4°–27.2°C (Fig. **F2B**). Short-term $SST_{Mg/Ca}$ fluctuations are on the order of 2°–2.5°C. A best fit to reveal long-term trends was calculated to show only variations on timescales longer than 185 k.y. (Fig. **F2**). The general trend in $SST_{Mg/Ca}$ shows warming (24.5°–25.5°C) between 4.8 and 3.7 Ma (Fig. **F2B**). After 3.7 Ma and more pronounced after 3.2 Ma, a cooling trend is apparent, paralleled by a continuous increase in $\delta^{18}O_{benthic}$ (**Tiedemann et al.,** this volume). This cooling after 3.2 Ma reflects irreversible intensification of NHG (Fig. **F2D**). Lowest $SST_{Mg/Ca}$ are recorded during marine isotope Stages (MIS) 96 and 100 (~2.5 Ma), when $SST_{Mg/Ca}$ dropped to values below 22°C. Highest $SST_{Mg/Ca}$ are recorded in samples older than 4.0 Ma, when maxima approached 27°C (Fig. **F2B**).

Applying spectral analysis to the Mg/Ca record reveals that the apparent 400-k.y. cycle in the older part of the record, which is suggested by the best fit, shows no relationship to the eccentricity cycle of 400 k.y. (Fig. **F3A**). Hence, we filtered the data sets to remove variations on timescales longer than 185 k.y, like intensification of NHG. In order to

F2. Results for Site 1241 for the time interval 4.8–2.4 Ma, p. 21.

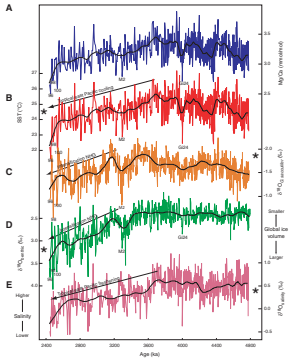

F3. Comparison of Mg/Ca and $\delta^{18}O_{G.sacculifer}$ with orbital parameters, p. 22.

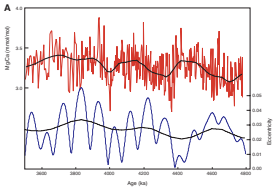

do so, we subtracted a best fit with a Gaussian window of 185 k.y. and a time step of 3 k.y. from the different records. Therefore, further results from spectral analyses are based on the detrended data sets.

The Mg/Ca record is dominated by a 41-k.y. cycle between 3.7 and 2.4 Ma (Fig. F4B), as expected, because of its increasing similarity to the $\delta^{18}O_{benthic}$ record (Figs. F2, F3B). The older part of the record (4.8 to 3.7 Ma) shows strong power at 100- and 23-k.y. periodicities and significantly reduced variance at 41-k.y. periodicity (Fig. F5B; Table T1). This suggests that regional low-latitude processes significantly contributed to the oceanography at Site 1241 during this period, as the presence of the 41-k.y. cycle, a typical high-latitude signal, is strongly reduced.

The $\delta^{18}O$ values of *G. sacculifer* vary between –0.8‰ and –2.18‰ with short-term fluctuations of ~0.5‰ (Fig. F2C). $\delta^{18}O_{G.sacculifer}$ values decrease from –1.5‰ to –1.85‰ from 4.8 to 3.5 Ma. A rapid increase toward MIS M2 at 3.3 Ma with a maximum of –0.8‰ and a subsequent decrease to –1.8‰ terminate the relatively warm interval of the Pliocene record. After 3.2 Ma, isotopic values increase, according to the global trend of intensification of NHG, and culminate at MIS 96, 98, and 100 (greater than –1.0‰) (Fig. F2C).

Spectral analysis of the $\delta^{18}O_{G.sacculifer}$ record between 3.7 and 2.4 Ma reveals dominant variability at the obliquity-related 41-k.y. cycle with significant power also in the 100-k.y. eccentricity band and little variability at precession-related cycles (Figs. F4C, F5C). Spectral variability in the older interval (4.8–3.7 Ma) is characterized by increased variance at precession-related cyclicities, similar to the Mg/Ca spectrum (Fig. F5C; Table T1).

We combined the $\delta^{18}O$ and Mg/Ca records of *G. sacculifer* to calculate variations in $\delta^{18}O_{water}$ (Shackleton, 1974). In the next step, we subtracted the Pliocene ice volume signal from the $\delta^{18}O_{water}$ record to assess relative variations in local SSS. Benway and Mix (2004) showed that the modern relationship between $\delta^{18}O_{water}$ and salinity in the Panama Bight is primarily controlled by variations in precipitation and its isotopic composition. An important source for the freshwater supply into the Panama Bight is the Caribbean, from where relatively ^{18}O-depleted rainfall is transported over the Isthmus of Panama. As the Pliocene configuration of the area was significantly different than today with the Panamanian Gateway still open, the relationship between $\delta^{18}O_{water}$ and salinity is not known, and, accordingly, we did not calculate absolute salinities. We used the $\delta^{18}O_{benthic}$ record of Site 1241 (**Tiedemann et al.,** this volume) to approximate Pliocene ice volume. The $\delta^{18}O_{benthic}$ difference between the Last Glacial Maximum (LGM) and the Holocene for the east Pacific is 1.6‰ (Shackleton et al., 1983), whereas the difference in global ice volume between the LGM and the Holocene is 1.0‰–1.2‰ (Fairbanks, 1989; Schrag et al., 1996), ~75% of the $\delta^{18}O_{benthic}$ signal for the east Pacific. We assumed that the relative contributions of ice volume, salinity, and temperature are also valid for the Pliocene. This would mean that the 1.1‰ amplitude for MIS 100 (Fig. F2D) reflects an ice volume signal of ~0.8‰, two-thirds of the LGM–Holocene ice volume difference (Raymo et al., 1989). When we take into account that it is likely that the isotopic composition of continental ice sheets has changed significantly since the Pliocene, a sea level change of 40–80 m can be expected for MIS 100 (Miller et al., 1987; Pekar et al., 2002). For our calculations, we used the maximum sea level change of 80 m (10 m sea level = 0.1‰ $\delta^{18}O$). The 1.1‰ amplitude in the

F4. Spectral analysis for the time interval 3.7–2.4 Ma, p. 24.

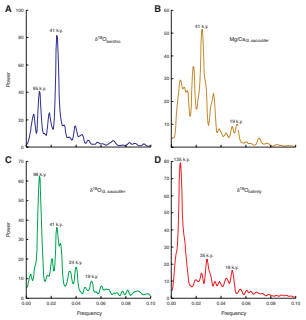

F5. Spectral analysis for the time interval 4.8–3.7 Ma, p. 25.

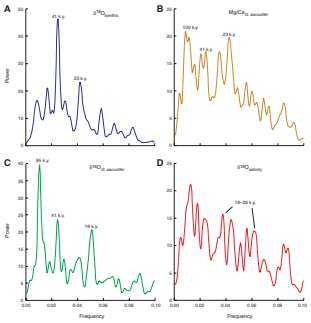

T1. Cross spectral analysis for Site 1241, p. 27.

$\delta^{18}O_{benthic}$ record for MIS 100 (Fig. F2D) was then normalized to an amplitude of 0.8‰ and accordingly extended to the entire $\delta^{18}O_{benthic}$ record. This normalized record was then subtracted from the $\delta^{18}O_{water}$ record, leaving a $\delta^{18}O_{salinity}$ record, which provides a first approximation of relative changes in local SSS (Fig. F2E). We are aware of the fact that this approach to assess SSS might be an oversimplification, but nevertheless it gives a reliable first approximation.

Prior to 3.7 Ma, the $\delta^{18}O_{salinity}$ record remains relatively constant around an average value of 0.55‰, with the exception of a decrease to 0.4‰ between 4.4 and 4.2 Ma (Fig. F2E). Between 3.7 and 3.6 Ma, average values decrease from 0.6‰ to 0.35‰. Between 3.6 and 2.7 Ma average values further decrease to 0.2‰, followed by a more pronounced decrease to –0.25‰ until 2.4 Ma. Spectral analysis of the $\delta^{18}O_{salinity}$ record indicates no power in the 41-k.y. frequency band, suggesting a decoupling from the global signal of the intensification of the NHG and high-latitude climate forcing (Fig. F4D). A weak precession signal for the entire time period indicates that local SSS is mainly controlled by low-latitude variations in the precipitation-evaporation budget instead of global, high-latitude forcing (Figs. F4D, F5D). This is corroborated by Benway and Mix (2004), who showed that surface water salinities in the Panama Bight are primarily determined by variations in rainfall, both originating from local sources as from the Caribbean.

MIXED-LAYER HYDROGRAPHY DURING THE EARLY PLIOCENE

The interval between 4.8 and 3.7 Ma reveals an increase in average $SST_{Mg/Ca}$ of 1°–1.5°C (Fig. F2B). Comparison with the $\delta^{18}O_{benthic}$ record (Fig. F2D), which indicates no significant trend during this period, shows that this increase in $SST_{Mg/Ca}$ cannot be correlated to a global warming trend. Therefore, the increase in $SST_{Mg/Ca}$ between 4.8 and 3.7 Ma represents regional warming. This suggests increased influence of the warm NECC and the ITCZ, as is also indicated by the $\delta^{18}O_{salinity}$ record. This might have been achieved either by the plate tectonic movement of Site 1241 toward a more northerly position (Mix, Tiedemann, Blum, et al., 2003) or to southward movement of the ITCZ/NECC.

A southward shift of the ITCZ during this period is supported by several other studies (Billups et al., 1999; Cannariato and Ravelo, 1997). On the other hand, it has also been suggested that the ITCZ remained at its position or even moved northward because of increasing heat piracy to the North Atlantic due to the progressive closure of the Panamanian Gateway (Tiedemann et al., 1989; Maier-Reimer et al., 1990; Haug and Tiedemann, 1998). This, then, would have strengthened the EUC, leading to a shallowing of the thermocline, as is also shown by **Steph et al.** (this volume). A shallowing of the thermocline might have led to a shallowing of the habitat depth of *G. sacculifer,* because *G. sacculifer* mainly lives in the mixed layer. A possible imprint on the SST reconstruction would have been a cooling trend because the whole upper water column is affected when the thermocline significantly shallows. However, our results do not show such a trend in the $SST_{Mg/Ca}$ record of *G. sacculifer* during this period. Therefore, we conclude that the shal-

lowing of the thermocline between 5.4 and 4.0 Ma had no or only minor effect on average SST in the mixed layer at the location of Site 1241.

The time interval between 4.8 and 3.7 Ma is further characterized by two significant cooling events at ~4.4–4.2 and 4.0 Ma (Fig. F2B). The event at 4.0 Ma can be clearly correlated with the $\delta^{18}O_{benthic}$ record and can be identified as MIS Gi24, representing a global cooling event. The event between 4.4 and 4.2 Ma, however, is not present in the $\delta^{18}O_{benthic}$ record and, therefore, possibly either signifies a regional cooling event or just an oscillation on the long-term trend. Possible explanations for this "event" include increasing southeast trade winds and a resulting northward movement of the ITCZ/NECC or increasing influence of cooler thermocline waters, as suggested by the shallowing thermocline and the progressive closure of the Panamanian Gateway.

Because the $\delta^{18}O_{benthic}$ record reveals no significant trend for the time period from 4.8 to 3.6 Ma (Fig. F2D), variations in the $\delta^{18}O_{G.sacculifer}$ and $\delta^{18}O_{salinity}$ records reflect a large portion of variance that has to be ascribed to changes in regional oceanography (Fig. F2C, F2E). The decrease in $\delta^{18}O_{G.sacculifer}$ from –1.5‰ to –1.8‰ (Fig. F2C) is explained by an increase in temperature, as is recorded by the Mg/Ca record (Fig. F2B). The $\delta^{18}O_{salinity}$ fluctuations (Fig. F2E) remain relatively constant during this period, except for the interval from 4.4 to 4.2 Ma, when average $\delta^{18}O_{salinity}$ values decrease to 0.4‰. This suggests that between 4.4 and 4.2 Ma Site 1241 bathed in a less saline water mass. This time interval corresponds with the main phase in the shallowing of the thermocline and is paralleled by a decrease in $SST_{Mg/Ca}$, suggesting increased influence of cooler thermocline waters or an increase in southeast trade winds and an intensified EUC. On the other hand, this would not result in decreasing SSS and $SST_{Mg/Ca}$ does not show any changes that can be correlated with the general shoaling of the thermocline. Less saline waters are associated with the tropical rainbelt (ITCZ). Increasing southeast trade winds would move the ITCZ toward the north. Therefore, it seems that this temporarily freshening is due to a a decrease in temperatures during this interval, changing the precipitation/evaporation ratio, causing less evaporation and lower saline waters. The synchronicity of this event with the critical threshold in the progressive closure of the Panamanian Gateway during this time might suggest a coupling between these events (Haug et al., 2001).

PERMANENT EL NIÑO?

The presence of a permanent El Niño-like Pliocene climate has been suggested by several authors (Molnar and Cane, 2002; Ravelo et al., 2004). During a present-day El Niño, the collapse of the easterlies leads to an equatorial Kelvin wave, which is characterized by the eastward flow of warm waters from the WPWP, leading to increasing SSTs in the east Pacific. In consequence, the temperature gradient between the WPWP and the east Pacific diminishes and the east Pacific thermocline deepens (Wallace et al., 1998, and references therein). Upwelling intensity, however, is not changing, but the upwelled water now comes from the warmer waters above the thermocline instead of below the thermocline (Barber and Chavez, 1983; McPhaden and Picaut, 1990). These changes significantly influence extratropical climates, for example, they cause warmer and wetter conditions in North America, drier conditions in southeast Asia and Australia, and drier conditions over north-

eastern South America (Molnar and Cane, 2002, and references therein). Several Pliocene reconstructions show extratropical conditions similar to those of the present-day El Niño (Zarate and Fasana, 1989; Dowsett and Poore, 1991; Wolfe, 1994; Archer et al., 1995). Evidence from the Pliocene tropical Pacific mainly comes from thermocline and SST gradient development. $\delta^{18}O$ records of *G. sacculifer* and foraminiferal faunal assemblages for the east and west Pacific show that the present-day SST gradient and the slope of the thermocline depth between the east and the west Pacific did not fully develop until 1.5 Ma (Chaisson, 1995; Cannariato and Ravelo, 1997; Chaisson and Ravelo, 2000; Ravelo et al., 2006), although a first and significant step toward a shallow thermocline occurred between 5.3 and 4.0 Ma (Ravelo et al., 2006; **Steph et al.,** this volume).

The areas which experience the largest SST anomalies in the east Pacific during El Niño events are the major upwellings areas along the coast of South America and along the equatorial divergence. Although the position of Site 1241 is, therefore, not the ideal place to record El Niño-related changes, SST anomalies associated with El Niño still show a warming of as much as 3°C during El Niño events (**www.cdc.noaa.gov**). Including the backtrack location of Site 1241 closer to the equatorial divergence, our data provide indications on the existence of a permanent El Niño-like climate during the Pliocene. The $SST_{Mg/Ca}$ record of *G. sacculifer,* however, does not show significantly higher temperatures for the early Pliocene in comparison with today, as would be expected. This result is also shown by Dowsett et al. (1996), who used foraminifer, diatom, and ostracode assemblages for a middle Pliocene time interval to reconstruct SSTs. However, they also show significant warming in mid and high latitudes, indicating that a globally warmer climate is not necessarily reflected by higher tropical Pacific SSTs, especially if the Pliocene atmospheric CO_2 concentrations were not significantly higher than modern ones (Van der Burgh et al., 1993). Present-day mixed-layer SSTs in the tropical east Pacific vary between 24° and 27°C for the upper 40 m (Levitus and Boyer, 1994), below which the thermocline starts. Taking into account the paleolocation of Site 1241 (Pisias et al., 1995; Mix, Tiedemann, Blum et al., 2003), SSTs would be expected to be lower by ~1°C for the early Pliocene. $SST_{Mg/Ca}$ for the early Pliocene indicates variations between 24° and 26.5°C for the habitat depth of *G. sacculifer.* A study by Lea et al. (2000) from the equatorial east Pacific (Core TR163-19, with a comparable position to the paleoposition of Site 1241), showed similar $SST_{Mg/Ca}$ fluctuations between 23° and 28°C for the surface-dwelling *Globigerinoides ruber* for the last 350 k.y. Since present-day SSTs are indicative of interglacial, maximum temperatures, we conclude that the tropical thermal maxima during the early Pliocene were not significantly different than modern interglacial SSTs. Therefore, our east Pacific $SST_{Mg/Ca}$ results do not directly support the idea of an early Pliocene permanent El Niño-like climate. An additional argument against a permanent El Niño-like climate is provided by the significant shallowing of the thermocline between 5.3 and 4.0 Ma (**Steph et al.,** this volume; Cannariato and Ravelo, 1997; Chaisson and Ravelo, 2000; Ravelo et al., 2006). On the other hand, a typical El Niño-like scenario with a decreased or even reversed east-west Pacific SST gradient might also have been caused by lower SSTs in the west Pacific, as was suggested by Cannariato and Ravelo (1997). Their estimation of SST, however, was based on $\delta^{18}O$ analyses, assuming no influence of salinity on $\delta^{18}O$. Andersson (1997) and Wang (1994) used

transfer functions on total planktonic foraminiferal assemblages to reconstruct Pliocene SSTs for the west Pacific. Their SST reconstructions, using three different transfer functions, showed SSTs similar to present SSTs in the west Pacific. Andersson (1997) actually investigated the difference between two transfer functions for cold and warm seasons for Ontong Java Plateau Ocean Drilling Program Site 806. All estimates were close to present SSTs and significantly higher than our average SSTs for the east Pacific (Fig. F6). Andersson's (1997) lowest estimate (Modern Analog technique) for the cold season was 27.0°C and the warmest estimate for the warm season (Imbrie-Kipp Transfer Function method) was 29.6°C, whereas our average $SST_{Mg/Ca}$ for the east Pacific is 24.7°C (Fig. F6). Although the age model of Andersson (1997) is not tuned to our age model, the general trends reveal a strong similarity between the two records between 4.0 and 3.2 Ma with the west Pacific constantly being warmer than the east Pacific by ~3°C. Further comparison between both SST records suggests a strengthening of the tropical west-east Pacific SST gradient along with major intensification of NHG after 3.2 Ma.

F6. Comparison between tropical east and west Pacific SSTs, p. 26.

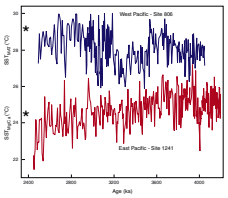

Therefore, we conclude that a "normal" SST gradient rather than a very weak, El Niño-like SST gradient between the west and the east Pacific seems more likely to have existed in the early Pliocene. Nevertheless, the closure of the Indonesian Gateway between 4.0 and 3.0 Ma (Cane and Molnar, 2001) and the decrease in east Pacific SST since 3.7 Ma might have played a role in further increasing the SST gradient toward present proportions.

INTENSIFICATION OF NHG

Between 4.8 and 3.4 Ma, the $\delta^{18}O_{benthic}$ record reveals no significant long-term trend, pointing to warm early Pliocene climate conditions without prominent changes in ice volume (Tiedemann et al., 1994). After 3.2 Ma, $\delta^{18}O_{benthic}$ increases from 2.5‰ to values of more than 3.5‰ for MIS 96, 98, and 100 at ~2.5 Ma. This increase, which can be globally observed, marks intensification of NHG (Ruddiman and Raymo, 1988; Raymo et al., 1989; Kwiek and Ravelo, 1999). The preceeding cooling trend (MIS M2; 3.4 to 3.3 Ma), as shown by the $\delta^{18}O_{benthic}$ and $SST_{Mg/Ca}$ records and which was abruptly terminated by the so-called mid-Pliocene warmth period (Crowley, 1996), may indicate a failed attempt of the climate system to start NHG (Haug and Tiedemann, 1998).

The decrease of $SST_{Mg/Ca}$ since 3.7 Ma starts several hundred thousand years earlier than the start of intensification of NHG at ~3.2 Ma as generally shown by global $\delta^{18}O_{benthic}$ records, which represent global ice volume (Lisiecki and Raymo, 2005). Average $SST_{Mg/Ca}$ decreases by ~2°C between 3.7 and 2.4 Ma. $\delta^{18}O_{G.sacculifer}$ increases by 0.8‰, which agrees with the change expected from the $SST_{Mg/Ca}$ decrease (2°C = ~0.5‰) and the ice volume effect of 0.4‰, which would give a total of 0.9‰.

Spectral analyses on the $SST_{Mg/Ca}$ record also indicate a change in spectral character at ~3.7 Ma. The interval from 4.8 to 3.7 Ma is characterized by a concentration of variance at eccentricity- and precession-related frequencies (Fig. F5B) with limited power at the 41-k.y. cycle. The interval from 3.7 to 2.4 Ma, comprising the tropical cooling trend in $SST_{Mg/Ca}$, in contrast, provides a strong 41-k.y. cycle and negligible variability at the precession band. The pronounced dominance of the 41-k.y. cycle after 3.7 Ma indicates that high-latitude climate forcing

has played an important role in driving SSTs in the tropical east Pacific because the presence of a strong obliquity related cycle typically reflects a high-latitude origin.

The similarity of the Mg/Ca and $\delta^{18}O$ records of *G. sacculifer* with the $\delta^{18}O_{benthic}$ record for the time period younger than 3.7 Ma is expressed by cross-spectral analysis between the proxies and the obliquity signal (Laskar, 1990) (Table T1). Coherency of all three proxies with obliquity exceeds 0.90 and coherency between $SST_{Mg/Ca}$ and $\delta^{18}O_{benthic}$ is 0.91, whereas none of the proxies significantly lags or leads obliquity. This suggests that the 41-k.y. rhythm in tropical east Pacific $\delta^{18}O_{benthic}$, $SST_{Mg/Ca}$, and $\delta^{18}O_{G.sacculifer}$ was mainly driven by variations of global importance, triggered by high-latitude processes that caused intensification of NHG (Figs. F3, F4).

Although the tropical cooling trend since 3.7 Ma is not reflected by an increase in ice volume before 3.4 Ma, evidence for early Pliocene high-latitude cooling is provided by sediment records from the Irminger and Norwegian Seas (Kleiven et al., 2002; St. John and Krissek, 2002). These records show significant pulses of ice-rafted debris back to 3.5 Ma, indicating the existence and development of glaciers large enough to produce icebergs well before intensification of NHG.

The warm Pliocene before intensification of NHG (Ravelo and Andreasen, 2000) is probably associated with atmospheric CO_2 concentrations that were higher than preindustrial concentrations by ~100 ppmv (Van der Burgh et al., 1993; Raymo et al., 1996). Although the mid-Pliocene warm period is generally assumed to have continued until 3.2 Ma, the initiation of an earlier decrease in atmospheric CO_2 cannot be excluded. Therefore, the lead of cooling tropical SSTs over the increase of global ice volume could indicate that a decrease in atmospheric CO_2 concentrations might have played an important role in intensification of NHG (Li et al., 1998). Decreasing atmospheric CO_2 concentrations would lead to global cooling, but global ice volume will not start to increase before a certain threshold is reached, thereby resulting in a lag of global ice volume to global temperatures (Raymo, 1998; DeConto and Pollard, 2003).

The expression of intensification of NHG is contradicted by Ravelo et al. (2004). The authors argued that the main phase of intensification of NHG is not linked to changes in the tropics, but rather to changes in the subtropics. The main changes in the tropics occurred between 4.5 and 4.0 Ma, simultaneously with the critical threshold in the shoaling of the Isthmus of Panama (Haug et al., 2001; Billups et al., 1999), and after 2.0 Ma, when the present-day SST gradient between the east and west Pacific became established (Cannariato and Ravelo, 1997; Chaisson and Ravelo, 2000). These changes also suggest that the main influence of the subtropics on the tropics, namely providing the source for cooler upwelling waters, did not develop until 2.0 Ma. If deepwater temperatures at high latitudes started to decrease during the middle Pliocene and then propagated toward the tropics, the thermocline would have to shallow in order to influence SSTs. However, the main phase of shallowing of the thermocline at Site 1241 ended around 4.0 Ma (**Steph et al.,** this volume), showing no significant changes around the period when $SST_{Mg/Ca}$ started to decrease at ~3.7 Ma (Fig. F2). From our data, we therefore conclude that intensification of NHG is paralleled by cooling in the tropical east Pacific, which even preceeded intensification of NHG by ~500 k.y.

The $\delta^{18}O_{salinity}$ record does not seem to show intensification of NHG. Instead of the expected trend toward higher salinity because of increasing global ice volume since 3.2 Ma, a freshening trend is present for this time period (Fig. F2E), which had already started at ~3.6 Ma when $SST_{Mg/Ca}$ also started to decrease. Also, the global obliquity signal of 41 k.y., which dominates the $\delta^{18}O_{benthic}$, $\delta^{18}O_{G.sacculifer}$, and Mg/Ca records, is not significant in the $\delta^{18}O_{salinity}$ record (Fig. F4D). This suggests that the variations in local SSS in the Pliocene east Pacific are mainly controlled by low-latitude processes and can be explained by changes in evaporation/precipitation that are most likely related to latitudinal variations in the tropical rainbelt (ITCZ) and the establishment of modern conditions (Benway and Mix, 2004) as a consequence of ongoing shoaling of the Isthmus of Panama. The average values of $\delta^{18}O_{salinity}$ for the time period 3.6 to 2.4 Ma are on average 0.4‰ lower than for the time period between 4.8 and 3.6 Ma, indicating generally fresher water masses at Site 1241. The present-day distribution of mixed-layer salinity in the east Pacific shows that lower saline water masses are related to the position of the ITCZ/NECC and the depth of the thermocline. Therefore, we conclude that between 3.6 and 2.4 Ma, mixed-layer water mass properties at Site 1241 became not only cooler but also less saline. This indicates that with intensification of NHG, the ITCZ possibly moved into a more southerly position with weaker southeast trade winds, a relatively weaker SEC and NECC, a strengthened EUC, and a shallower thermocline in comparison with the period from 4.8 to 3.6 Ma.

CONCLUSIONS

High-resolution analyses of the mixed-layer dwelling planktonic foraminifer *G. sacculifer* for Mg/Ca and $\delta^{18}O$ for Site 1241 reveal the development of east Pacific surface hydrography for the time interval from 4.8 to 2.4 Ma.

An increase in average $SST_{Mg/Ca}$ (24.5°–25.5°C) between 4.8 and 3.7 Ma interrupted by short-term cooler periods, can be explained by a general southward shift of the ITCZ, increasing the influence of the warmer NECC.

The general global cooling trend, a response to intensification of NHG started at ~3.2 Ma, shown by the $\delta^{18}O_{benthic}$ record, is paralleled by tropical east Pacific cooling, indicated by $SST_{Mg/Ca}$. Tropical east Pacific cooling, however, had already commenced around 3.7 Ma, suggesting that global cooling, probably related to decreasing atmospheric CO_2 concentrations, might have started well before intensification of NHG.

Relative variations in local SSS indicated by $\delta^{18}O_{salinity}$ show a decoupling from the global, high-latitude processes shown by the $\delta^{18}O_{benthic}$ record. Long-term regional freshening started with decreasing $SST_{Mg/Ca}$ at ~3.7 Ma, suggesting that changes in the tropical wind field in combination with latitudinal shifts of the tropical rainbelt related with general decrease in tropical east Pacific SST–controlled $\delta^{18}O_{salinity}$.

Pliocene $SST_{Mg/Ca}$ for *G. sacculifer* for Site 1241 close to modern SSTs in the tropical east Pacific, in combination with the early Pliocene development of a shallow thermocline, give no direct support to the idea that a permanent El Niño-like Pliocene climate might have existed during the early Pliocene.

ACKNOWLEDGMENTS

We would like to thank S. Koch, K. Wittmaack, N. Gau, A. Jesussek, U. Nielsen, and K. Kissling for sample preparation and laboratory assistance. J. Groeneveld especially thanks M. Greaves and H. Elderfield (Cambridge University) for introduction into Mg/Ca analyses. We thank C. Andersson Dahl for providing the data for Figure F6. We also gratefully thank A. Mix, W. F. Ruddiman, and one anonymous reviewer for their useful comments. This research used samples and data provided by the Ocean Drilling Program (ODP). ODP is sponsored by the U.S. National Science Foundation (NSF) and participating countries under management of Joint Oceanographic Institutions (JOI), Inc. This study was performed within DFG-Research Unit, FOR 451 (Impact of Gateways on Ocean Circulation, Climate, and Evolution; funding under Ti240/12-2).

REFERENCES

Andersson, C., 1997. Transfer function vs. modern analog technique for estimating Pliocene sea-surface temperatures based on planktonic foraminiferal data, western equatorial Pacific Ocean. *J. Foraminiferal Res.,* 27:123–132.

Archer, M., Hand, S.J., and Godthelp, H., 1995. Tertiary environmental and biotic change in Australia. *In* Vrba, E.S., Denton, G.H., Partridge, T.C., and Burckle, L.H. (Eds.), *Paleoclimate and Evolution, with Emphasis on Human Origins:* New Haven (Yale Univ. Press), 77–90.

Barber, R.T., and Chavez, F.P., 1983. Biological consequences of El Niño. *Science,* 222:1203–1210.

Barker, S., Greaves, M., and Elderfield, H., 2003. A study of cleaning procedures used for foraminiferal Mg/Ca paleothermometry. *Geochem., Geophys., Geosyst.,* 4(9):8407. **doi:10.1029/2003GC000559**

Benway, H.M., and Mix, A.C., 2004. Oxygen isotopes, upper-ocean salinity, and precipitation sources in the eastern tropical Pacific. *Earth Planet. Sci. Lett.,* 224(3–4):493–507. **doi:10.1016/j.epsl.2004.05.014**

Berner, R.A., Lasaga, A.C., and Garrels, R.M., 1983. The carbonate-silicate geochemical cycle and its effect on atmospheric carbon dioxide over the past 100 million years. *Am. J. Sci.,* 283:641–683.

Billups, K., Ravelo, A.C., Zachos, J.C., and Norris, R.D., 1999. Link between oceanic heat transport, thermohaline circulation, and the Intertropical Convergence Zone in the early Pliocene Atlantic. *Geology,* 27(4):319–322. **doi:10.1130/0091-7613(1999)027<0319:LBOHTT>2.3.CO;2**

Broecker, W.S., and Peng, T.-H., 1982. *Tracers in the Sea:* Palisades, NY (Eldigio Press).

Brown, S.J., 1996. Controls on the trace metal chemistry of foraminiferal calcite and aragonite [Ph.D. dissert.]. Univ. of Cambridge, UK.

Cane, M.A., and Molnar, P., 2001. Closing of the Indonesian Seaway as a precursor to East African aridification around 3–4 million years ago. *Nature (London, U. K.),* 411(6834):157–162. **doi:10.1038/35075500**

Cannariato, K.G., and Ravelo, A.C., 1997. Pliocene–Pleistocene evolution of the eastern tropical Pacific surface water circulation and thermocline depth. *Paleoceanography,* 12(6):805–820. **doi:10.1029/97PA02514**

Chaisson, W., 1995. Planktonic foraminiferal assemblages and paleoceanographic change in the trans-tropical Pacific Ocean: a comparison of west (Leg 130) and east (Leg 138), latest Miocene to Pleistocene. *In* Pisias, N.G., Mayer, L.A., Janecek, T.R., Palmer-Julson, A., and van Andel, T.H. (Eds.), *Proc. ODP, Sci. Results,* 138: College Station, TX (Ocean Drilling Program), 555–597.

Chaisson, W.P., and Ravelo, A.C., 2000. Pliocene development of the east–west hydrographic gradient in the equatorial Pacific. *Paleoceanography,* 15(5):497–505. **doi:10.1029/1999PA000442**

Crowley, T.J., 1996. Pliocene climates: the nature of the problem. *Mar. Micropaleontol.,* 27(1–4):3–12. **doi:10.1016/0377-8398(95)00049-6**

Curry, W.B., Thunell, R.C., and Honjo, S., 1983. Seasonal changes in the isotopic composition of planktonic foraminifera collected in Panama Basin sediment traps. *Earth Planet. Sci. Lett.,* 64(1):33–43. **doi:10.1016/0012-821X(83)90050-X**

DeConto, R.M., and Pollard, D., 2003. Rapid Cenozoic glaciation of Antarctica induced by declining atmospheric CO_2. *Nature (London, U. K.),* 421(6920):245–249. **doi:10.1038/nature01290**

Donguy, J.R., and Meyers, G., 1996. Mean annual variation of transport of major currents in the tropical Pacific Ocean. *Deep-Sea Res., Part I,* 43(7):1105–1122. **doi:10.1016/0967-0637(96)00047-7**

Dowsett, H.J., and Poore, R.Z., 1991. Pliocene sea surface temperatures of the North Atlantic Ocean at 3.0 Ma. *In* Cronin, T.M., and Dowsett, H.J. (Eds.), *Pliocene Climates*. Quat. Sci. Rev., 10(2–3):189–204. **doi:10.1016/0277-3791(91)90018-P**

Dowsett, H.J., Barron, J., and Poore, R., 1996. Middle Pliocene sea surface temperatures: a global reconstruction. *Mar. Micropaleontol.,* 27(1–4):13–15. **doi:10.1016/0377-8398(95)00050-X**

Elderfield, H., and Schultz, A., 1996. Mid-ocean ridge hydrothermal fluxes and the chemical composition of the ocean. *Annu. Rev. Earth Planet. Sci.,* 24(1):191–224. **doi:10.1146/annurev.earth.24.1.191**

Elderfield, H., Vautravers, M., and Cooper, M., 2002. The relationship between shell size and Mg/Ca, Sr/Ca, $\delta^{18}O$ and $\delta^{13}C$ of species of planktonic foraminifera. *Geochem., Geophys., Geosyst.,* 3(8):1052. **doi:10.1029/2001GC000194**

Fairbanks, R.G., 1989. A 17,000-year glacio-eustatic sea level record: influence of glacial melting rates on the Younger Dryas event and deep-ocean circulation. *Nature (London, U. K.),* 342:637–642. **doi:10.1038/342637a0**

Fairbanks, R.G., Sverdlove, M., Free, R., Wiebe, P.H., and Bé, A.W.H., 1982. Vertical distribution and isotopic fractionation of living planktonic foraminifera from the Panama Basin. *Nature (London, U. K.),* 298:841–844. **doi:10.1038/298841a0**

Fedorov, A.V., Dekens, P.S., McCarthy, M., Ravelo, A.C., deMenocal, P.B., Barreiro, M., Pacanowski, R.C., and Philander, S.G., 2006. The Pliocene paradox (mechanisms for a permanent El Niño). *Science,* 312(5779):1485–1489. **doi:10.1126/science.1122666**

Gieskes, J.M., and Lawrence, J.R., 1981. Alteration of volcanic matter in deep-sea sediments: evidence from the chemical composition of interstitial waters from deep sea drilling cores. *Geochim. Cosmochim. Acta,* 45(10):1687–1703.

Halpern, D., and Weisberg, R.H., 1989. Upper ocean thermal and flow fields at 0°, 28°W (Atlantic) and 0°, 140°W (Pacific) during 1983–1985. *Deep-Sea Res., Part I,* 36(3):407–418. **doi:10.1016/0198-0149(89)90044-7**

Haug, G.H., and Tiedemann, R., 1998. Effect of the formation of the Isthmus of Panama on Atlantic Ocean thermohaline circulation. *Nature (London, U. K.),* 393(6686):673–676. **doi:10.1038/31447**

Haug, G.H., Tiedemann, R., Zahn, R., and Ravelo, A.C., 2001. Role of Panama uplift on oceanic freshwater balance. *Geology,* 29(3):207–210. **doi:10.1130/0091-7613(2001)029<0207:ROPUOO>2.0.CO;2**

Huber, M., 2002. Straw man 1: a preliminary view of the tropical Pacific from a global coupled climate model simulation of the early Paleogene. *In* Lyle, M., Wilson, P.A., Janecek, T.R., et al., *Proc. ODP, Init. Repts.,* 199: College Station, TX (Ocean Drilling Program), 1–30. **doi:10.2973/odp.proc.ir.199.103.2002**

Keigwin, L., 1982. Isotopic paleoceanography of the Caribbean and east Pacific: role of Panama uplift in late Neogene time. *Science,* 217:350–353.

Kleiven, H.F., Jansen, E., Fronval, T., and Smith, T.M., 2002. Intensification of Northern Hemisphere glaciations in the circum Atlantic region (3.5–2.4 Ma)—ice-rafted detritus evidence. *Palaeogeogr., Palaeoclimatol., Palaeoecol.,* 184(3–4):213–223. **doi:10.1016/S0031-0182(01)00407-2**

Kwiek, P.B., and Ravelo, A.C., 1999. Pacific Ocean intermediate and deep water circulation during the Pliocene. *Palaeogeogr., Palaeoclimatol., Palaeocol.,* 154(3):191–217. **doi:10.1016/S0031-0182(99)00111-X**

Laskar, J., 1990. The chaotic motion of the solar system: a numerical estimate of the size of the chaotic zones. *Icarus,* 88(2):266–291. **doi:10.1016/0019-1035(90)90084-M**

Lea, D.W., Martin, P.A., Pak, D.K., and Spero, H.J., 2002. Reconstructing a 350 k.y. history of sea level using planktonic Mg/Ca and oxygen isotope records from a Cocos Ridge core. *Quat. Sci. Rev.,* 21(1–3):283–293. **doi:10.1016/S0277-3791(01)00081-6**

Lea, D.W., Pak, D.K., and Spero, H.J., 2000. Climate impact of late Quaternary equatorial Pacific sea surface temperature variations. *Science,* 289(5485):1719–1724. **doi:10.1126/science.289.5485.1719**

Levitus, S., and Boyer, T.P., 1994. *World Ocean Atlas 1994* (Vol. 4): *Temperature*. NOAA Atlas NESDIS 4.

Li, X.S., Berger, A., Loutre, M.F., Maslin, M.A., Haug, G.H., and Tiedemann, R., 1998. Simulating late Pliocene Northern Hemisphere climate with the LLN 2-D model. *Palaeogeogr., Palaeoclimatol., Palaoeocol.,* 25(6):915–918.

Lisiecki, L.E., and Raymo, M.E., 2005. A Pliocene–Pleistocene stack of 57 globally distributed benthic $\delta^{18}O$ records. *Paleoceanography,* 20(1):PA1003. **doi:10.1029/2004PA001071**

Lyle, M., Dadey, K.A., and Farrell, J.W., 1995. The late Miocene (11–8 Ma) eastern Pacific carbonate crash: evidence for reorganization of deep-water circulation by the closure of the Panama Gateway. *In* Pisias, N.G., Mayer, L.A., Janecek, T.R., Palmer-Julson, A., and van Andel, T.H. (Eds.), *Proc. ODP, Sci. Results,* 138: College Station, TX (Ocean Drilling Program), 821–838.

Maier-Reimer, E., Mikolajewicz, U., and Crowley, T., 1990. Ocean general circulation model sensitivity experiment with an open Central American isthmus. *Paleoceanography,* 5:349–366.

McPhaden, M.J., and Picaut, J., 1990. El Niño–southern oscillation displacements of the western equatorial Pacific warm pool. *Science,* 250:1385–1388.

Miller, K., Fairbanks, R., and Mountain, G., 1987. Tertiary oxygen isotope synthesis, sea level history, and continental margin erosion. *Paleoceanography,* 2:1–19.

Mitchell, T.P., and Wallace, J.M., 1992. The annual cycle of equatorial convection and sea surface temperature. *J. Clim.,* 5(10):1140–1156. **doi:10.1175/1520-0442(1992)005<1140:TACIEC>2.0.CO;2**

Mix, A.C., Tiedemann, R., Blum, P., et al., 2003. *Proc. ODP, Init. Repts.,* 202: College Station, TX (Ocean Drilling Program). **doi:10.2973/odp.proc.ir.202.2003**

Molnar, P., and Cane, M.A., 2002. El Niño's tropical climate and teleconnections as a blueprint for pre-Ice Age climates. *Paleoceanography,* 17(2):1021. **doi:10.1029/2001PA000663**

Mottl, M.J., and Wheat, C.G., 1994. Hydrothermal circulation through mid-ocean ridge flanks: fluxes of heat and magnesium. *Geochim. Cosmochim. Acta,* 58(10):2225–2237.

Nürnberg, D., 2000. Paleoclimate: taking the temperature of past ocean surfaces. *Science,* 289(5485):1698–1699. **doi:10.1126/science.289.5485.1698**

Nürnberg, D., Müller, A., and Schneider, R.R., 2000. Paleo-sea surface temperature calculations in the equatorial east Atlantic from Mg/Ca ratios in planktic foraminifers: a comparison to sea surface temperature estimates from $U_{37}^{K'}$, oxygen isotopes, and foraminiferal transfer function. *Paleoceanography,* 15(1):124–134. **doi:10.1029/1999PA000370**

Paillard, D., Labeyrie, L., and Yiou, P., 1996. Macintosh program performs time-series analysis. *Eos, Trans. Am. Geophys. Union,* 77:379.

Pekar, S.F., Christie-Blick, N., Kominz, M.A., and Miller, K.G., 2002. Calibration between eustatic estimates from backstripping and oxygen isotopic records for the Oligocene. *Geology,* 30(10):903–906. **doi:10.1130/0091-7613(2002)030<0903:CBEEFB>2.0.CO;2**

Pisias, N.G., Mayer, L.A., and Mix, A.C., 1995. Paleoceanography of the eastern equatorial Pacific during the Neogene: synthesis of Leg 138 drilling results. *In* Pisias, N.G., Mayer, L.A., Janecek, T.R., Palmer-Julson, A., and van Andel, T.H. (Eds.), *Proc. ODP, Sci. Results,* 138: College Station, TX (Ocean Drilling Program), 5–21.

Ravelo, A.C., and Andreasen, D.H., 2000. Enhanced circulation during a warm period. *Geophys. Res. Lett.,* 27(7):1001–1004. **doi:10.1029/1999GL007000**

Ravelo, A.C., Andreasen, D.H., Lyle, M., Lyle, A.O., and Wara, M.W., 2004. Regional climate shifts caused by gradual global cooling in the Pliocene epoch. *Nature (London, U. K.),* 429(6989):263–267. **doi:10.1038/nature02567**

Ravelo, A.C., Dekens, P.S., and McCarthy, M., 2006. Evidence for El Niño-like conditions during the Pliocene. *GSA Today,* 16(3):4–11. **doi:10.1130/1052-5173(2006)016<4:EFENLC>2.0.CO;2**

Ravelo, A.C., and Shackleton, N.J., 1995. Evidence for surface-water circulation changes at Site 851 in the eastern tropical Pacific. *In* Pisias, N.G., Mayer, L.A., Jan-

ecek, T.R., Palmer-Julson, A., and van Andel, T.H. (Eds.), *Proc. ODP, Sci. Results,* 138: College Station, TX (Ocean Drilling Program), 503–514.

Raymo, M.E., 1998. Glacial puzzles. *Science,* 281:1467–1468.

Raymo, M.E., Grant, B., Horowitz, M., and Rau, G.H., 1996. Mid-Pliocene warmth: stronger greenhouse and stronger conveyor. *Mar. Micropaleontol.,* 27(1–4):313–326. **doi:10.1016/0377-8398(95)00048-8**

Raymo, M.E., Ruddiman, W.F., Backman, J., Clement, B.M., and Martinson, D.G., 1989. Late Pliocene variation in Northern Hemisphere ice sheets and North Atlantic deep water circulation. *Paleoceanography,* 4:413–446.

Ries, J.B., 2004. Effect of ambient Mg/Ca ratio on Mg fractionation in calcareous marine invertebrates: a record of the oceanic Mg/Ca ratio over the Phanerozoic. *Geology,* 32(11):981–984. **doi:10.1130/G20851.1**

Ruddiman, W.F., and Raymo, M.E., 1988. Northern Hemisphere climatic regimes during the past 3 Ma: possible tectonic connections. *Philos. Trans. R. Soc. London, Ser. B,* 318:411–430.

Schmidt, M.W., Spero, H.J., and Lea, D.W., 2004. Links between salinity variation in the Caribbean and North Atlantic thermohaline circulation. *Nature (London, U. K.),* 428(6979):160–163. **doi:10.1038/nature02346**

Schrag, D.P., Hampt, G., and Murray, D.W., 1996. Pore fluid constraints on the temperature and oxygen isotopic composition of the glacial ocean. *Science,* 272:1930–1932.

Shackleton, N.J., 1974. Attainment of isotopic equilibrium between ocean water and the benthonic foraminifera genus *Uvigerina:* isotopic changes in the ocean during the last glacial. *Les Meth. Quant. d'etude Var. Clim. au Cours du Pleist., Coll. Int. CNRS.,* 219:203–209.

Shackleton, N.J., Hall, M.A., and Pate, D., 1995. Pliocene stable isotope stratigraphy of Site 846. *In* Pisias, N.G., Mayer, L.A., Janecek, T.R., Palmer-Julson, A., and van Andel, T.H. (Eds.), *Proc. ODP, Sci. Results,* 138: College Station, TX (Ocean Drilling Program), 337–355.

Shackleton, N.J., Imbrie, J., and Hall, M.A., 1983. Oxygen and carbon isotope record of east Pacific Core V19-30: implications for the formation of deep water in the late Pleistocene North Atlantic. *Earth Planet. Sci. Lett.,* 65(2):233–244. **doi:10.1016/0012-821X(83)90162-0**

Shevenell, A.E., Kennett, J.P., and Lea, D.W., 2004. Middle Miocene Southern Ocean cooling and Antarctic cryosphere expansion. *Science,* 305(5691):1766–1770. **doi:10.1126/science.1100061**

Stanley, S.M., and Hardie, L.A., 1998. Secular oscillations in the carbonate mineralogy of reef-building and sediment-producing organisms driven by tectonically forced shifts in seawater chemistry. *Palaeogeogr., Palaeoclimatol., Palaeoecol.,* 144(1–2):3–19. **doi:10.1016/S0031-0182(98)00109-6**

St. John, K.E.K., and Krissek, L.A., 2002. The late Miocene to Pleistocene ice-rafting history of southeast Greenland. *Boreas,* 31(1):28–35. **doi:10.1080/03009480210651**

Tiedemann, R., and Franz, S.O., 1997. Deep-water circulation, chemistry, and terrigenous sediment supply in the equatorial Atlantic during the Pliocene, 3.3–2.6 Ma and 5–4.5 Ma. *In* Shackleton, N.J., Curry, W.B., Richter, C., and Bralower, T.J. (Eds.), *Proc. ODP, Sci. Results,* 154: College Station, TX (Ocean Drilling Program), 299–318.

Tiedemann, R., Sarnthein, M., and Shackleton, N.J., 1994. Astronomic timescale for the Pliocene Atlantic $\delta^{18}O$ and dust flux records of Ocean Drilling Program Site 659. *Paleoceanography,* 9(4):619–638.

Tiedemann, R., Sarnthein, M., and Stein, R., 1989. Climatic changes in the western Sahara: aeolo-marine sediment record of the last 8 million years (Sites 657–661). *In* Ruddiman, W., Sarnthein, M., et al., *Proc. ODP, Sci. Results,* 108: College Station, TX (Ocean Drilling Program), 241–277. **doi:10.2973/odp.proc.sr.108.169.1989**

Tripati, A.K., Delaney, M.L., Zachos, J.C., Anderson, L.D., Kelly, D.C., and Elderfield, H., 2003. Tropical sea-surface temperature reconstruction for the early Paleogene

using Mg/Ca ratios of planktonic foraminifera. *Paleoceanography,* 18(4):1101. doi:10.1029/2003PA000937

Umatani, S., and Yamagata, T., 1991. Response of the eastern tropical Pacific to meridional migration of the ITCZ: the generation of the Costa Rica dome. *J. Phys. Oceanogr.,* 21(2):346–363. doi:10.1175/1520-0485(1991)021<0346:ROTETP>2.0.CO;2

Van der Burgh, J., Visscher, H., Dilcher, D.L., and Kürschner, W.M., 1993. Paleoatmospheric signatures in Neogene fossil leaves. *Science,* 260:1788–1790.

Wallace, J.M., Rasmusson, E.M., Mitchell, T.P., Kousky, V.E., Sarachik, E.S., and von Storch, H., 1998. On the structure and evolution of ENSO-related climate variability in the tropical Pacific: lessons from TOGA. *J. Geophys. Res.,* 103(C7):14241–14259. doi:10.1029/97JC02905

Wang, C., and Enfield, D.B., 2001. The tropical Western Hemisphere warm pool. *Geophys. Res. Lett.,* 28(8):1635–1638. doi:10.1029/2000GL011763

Wang, L., 1994. Sea surface temperature history of the low latitude western Pacific during the last 5.3 million years. *Palaeogeogr., Palaeoclimatol., Palaeoecol.,* 108:379–436.

Weyl, P.K., 1968. The role of the oceans in climatic change: a theory of the ice ages. *Meteorol. Monogr.,* 8:37–62.

Wilkinson, B.H., and Algeo, T.J., 1989. Sedimentary carbonate record of calcium-magnesium cycling. *Am. J. Sci.,* 289:1158–1194.

Wolfe, J.A., 1994. An analysis of Neogene climates in Beringia. *Palaeogeogr., Palaeoclimatol., Palaeoecol.,* 108(3–4):207–216. doi:10.1016/0031-0182(94)90234-8

Xie, S.-P., Xu, H., Kessler, W.S., and Nonaka, M., 2005. Air-sea interaction over the eastern Pacific warm pool: gap winds, thermocline dome, and atmospheric convection. *J. Clim.,* 18(1):5–20. doi:10.1175/JCLI-3249.1

Zarate, M.A., and Fasano, J.L., 1989. The Plio–Pleistocene record of the central eastern Pampas, Buenos Aires province, Argentina: the Chapadmalal case study. *Palaeogeogr., Palaeoclimatol., Palaeoecol.,* 72:27–52. doi:10.1016/0031-0182(89)90130-2

Zaucker, F., Stocker, T.F., and Broecker, W.S., 1994. Atmospheric freshwater fluxes and their effect on the global thermohaline circulation. *J. Geophys. Res.,* 99(C6):12443–12458. doi:10.1029/94JC00526

Figure F1. Present-day (**A**) SST and (**B**) SSS distribution for the tropical eastern Pacific with the major currents and their flow directions as well as the location of Site 1241 (5°50′N, 86°26′W). Paleolocation (open circle) of Site 1241 is backtracked to 3°N, 87.7°W (Mix, Tiedemann, Blum, et al., 2003). Arrows indicate the flow direction of the following currents: NEC = North Equatorial Current, NECC = North Equatorial Countercurrent, SEC = South Equatorial Current, EUC = Equatorial Undercurrent, PCC = Peru-Chile Current. SSTs and SSSs are according to Levitus and Boyer (1994) at a water depth of 30 m. Dotted lines indicate the average annual position of the Intertropical Convergence Zone (ITCZ).

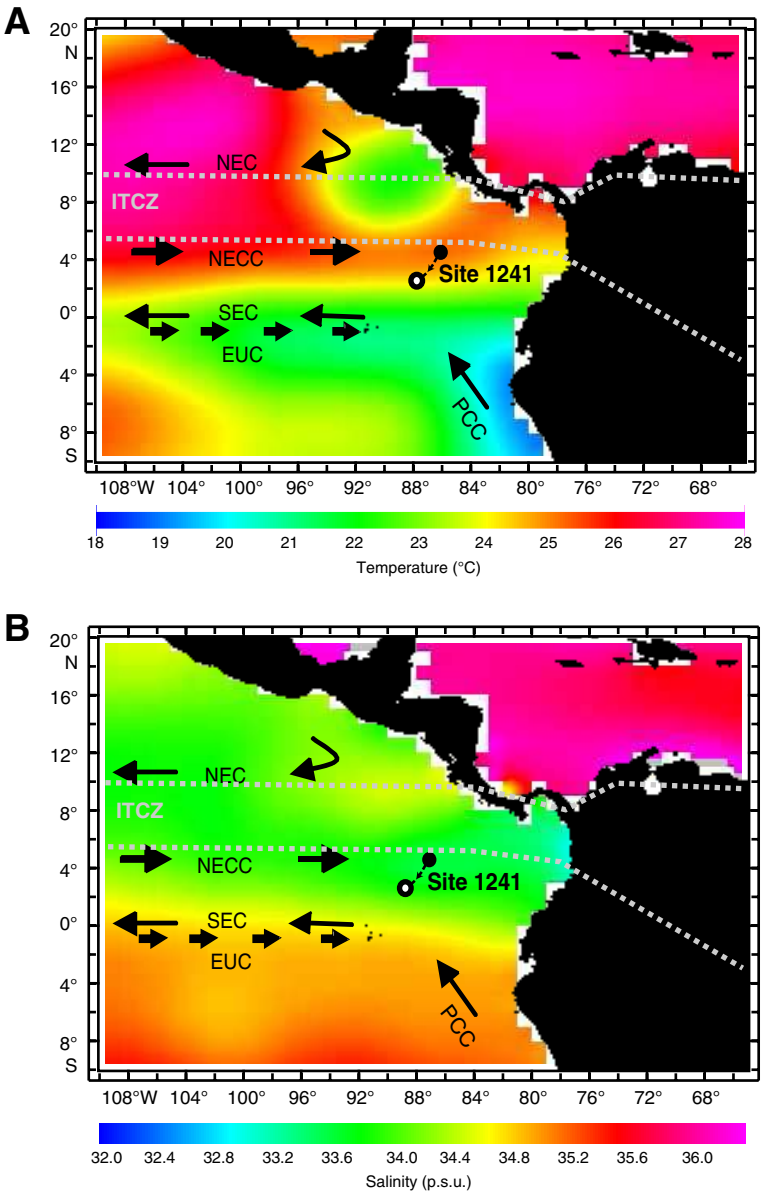

Figure F2. Results for Site 1241 for the time interval 4.8–2.4 Ma. **A.** Mg/Ca ratios, measured in foraminiferal tests of the planktonic foraminifer *Globigerinoides sacculifer.* **B.** Sea-surface temperatures (SSTs), calculated from the $Mg/Ca_{G.sacculifer}$ ratios using the equation of Nürnberg et al. (2000). **C.** $\delta^{18}O$, measured in foraminiferal tests of the planktonic foraminifer *G. sacculifer.* **D.** $\delta^{18}O$, measured on benthic foraminifers (**Tiedemann et al.,** this volume). **E.** $\delta^{18}O_{salinity}$, calculated by subtracting the normalized $\delta^{18}O_{benthic}$ record from the $\delta^{18}O_{water}$ record. Arrows indicate trends associated with intensification of Northern Hemisphere glaciation (NHG) and the tropical cooling and freshening in the east Pacific. Thick curved lines represent best fits on the data, showing variations on timescales >185 k.y. Numbers 96, 98, 100, M2, and Gi24 indicate marine isotope stages, according to the isotope nomenclature of Shackleton et al. (1995). * = modern property values at the paleolocation of Site 1241 (Levitus and Boyer, 1994).

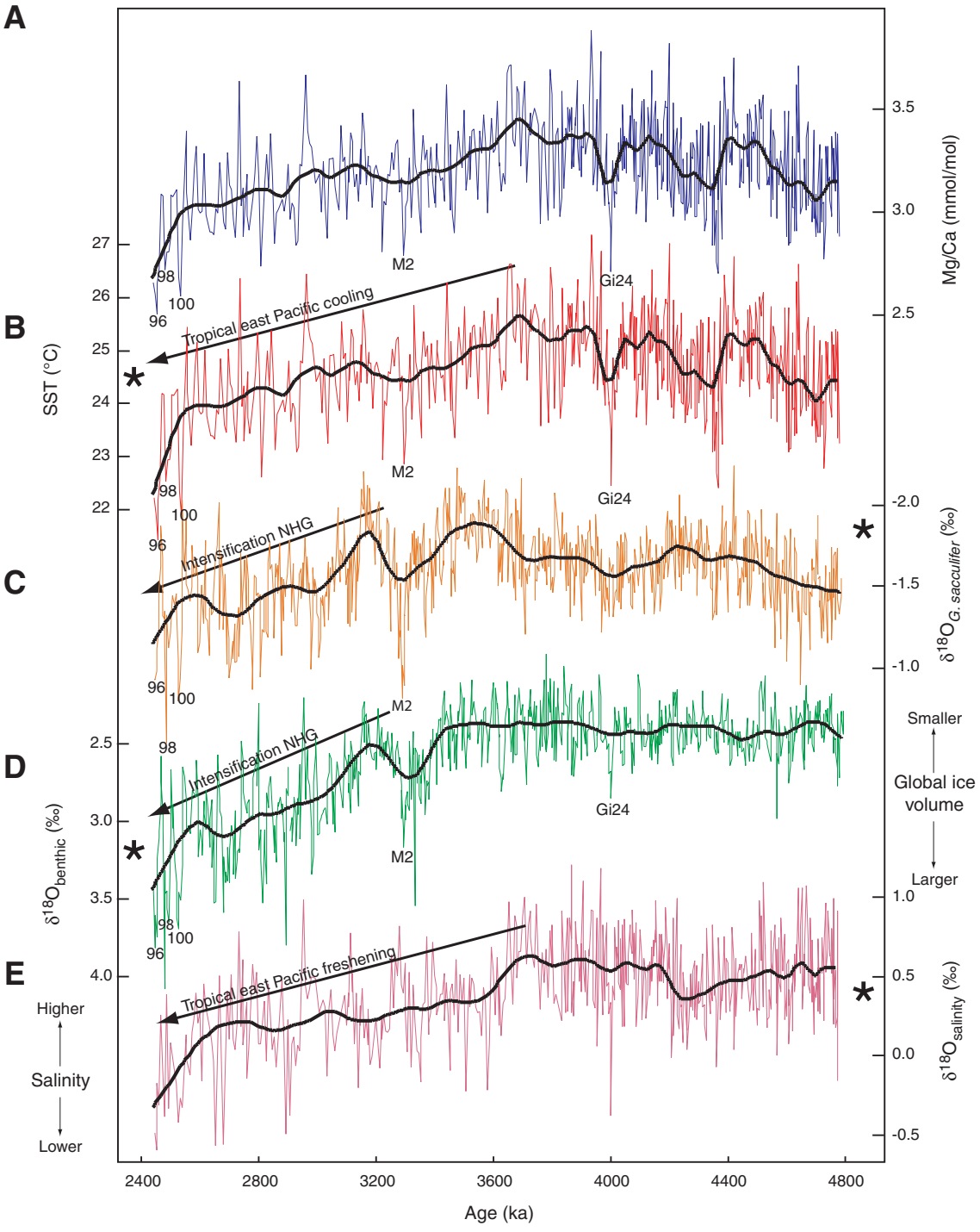

Figure F3. Comparison of Mg/Ca and $\delta^{18}O_{G.sacculifer}$ with orbital parameters (Laskar, 1990). **A.** Comparison of Mg/Ca with eccentricity for the time interval 4.8–3.5 Ma. (Continued on next page.)

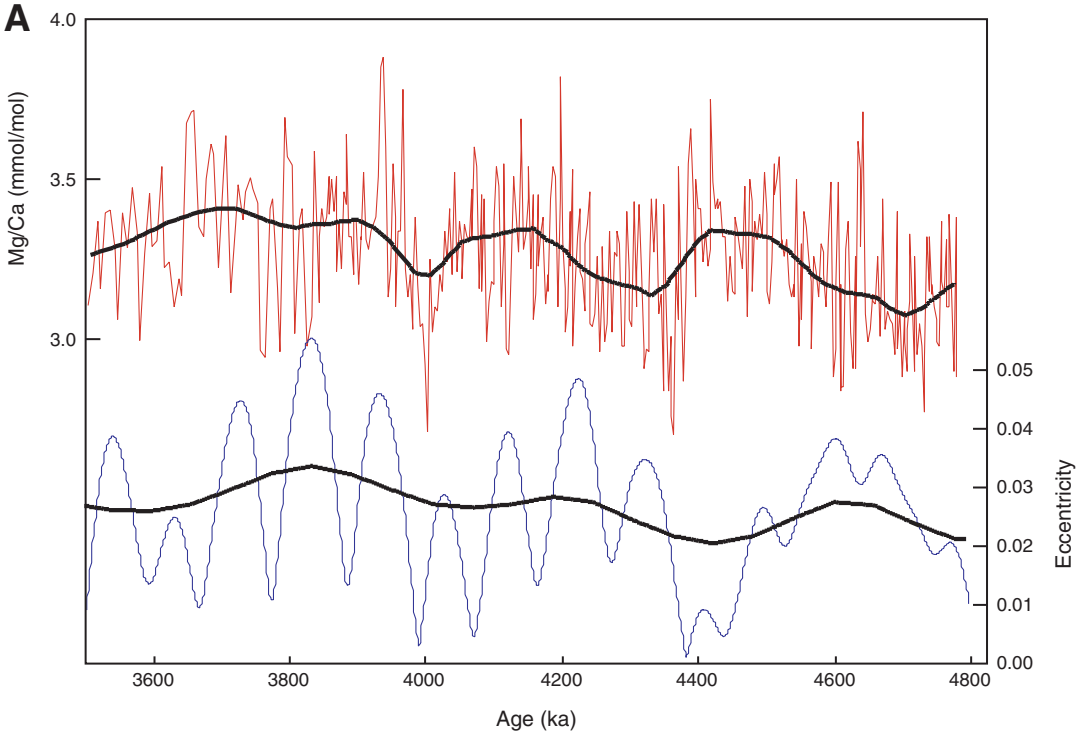

Figure F3 (continued). B. Comparison of Mg/Ca and $\delta^{18}O_{G.sacculifer}$ with obliquity for the time interval 3.7–2.4 Ma. Mg/Ca and $\delta^{18}O_{G.sacculifer}$ are shown as detrended (variations >185 k.y. are filtered) and normalized curves.

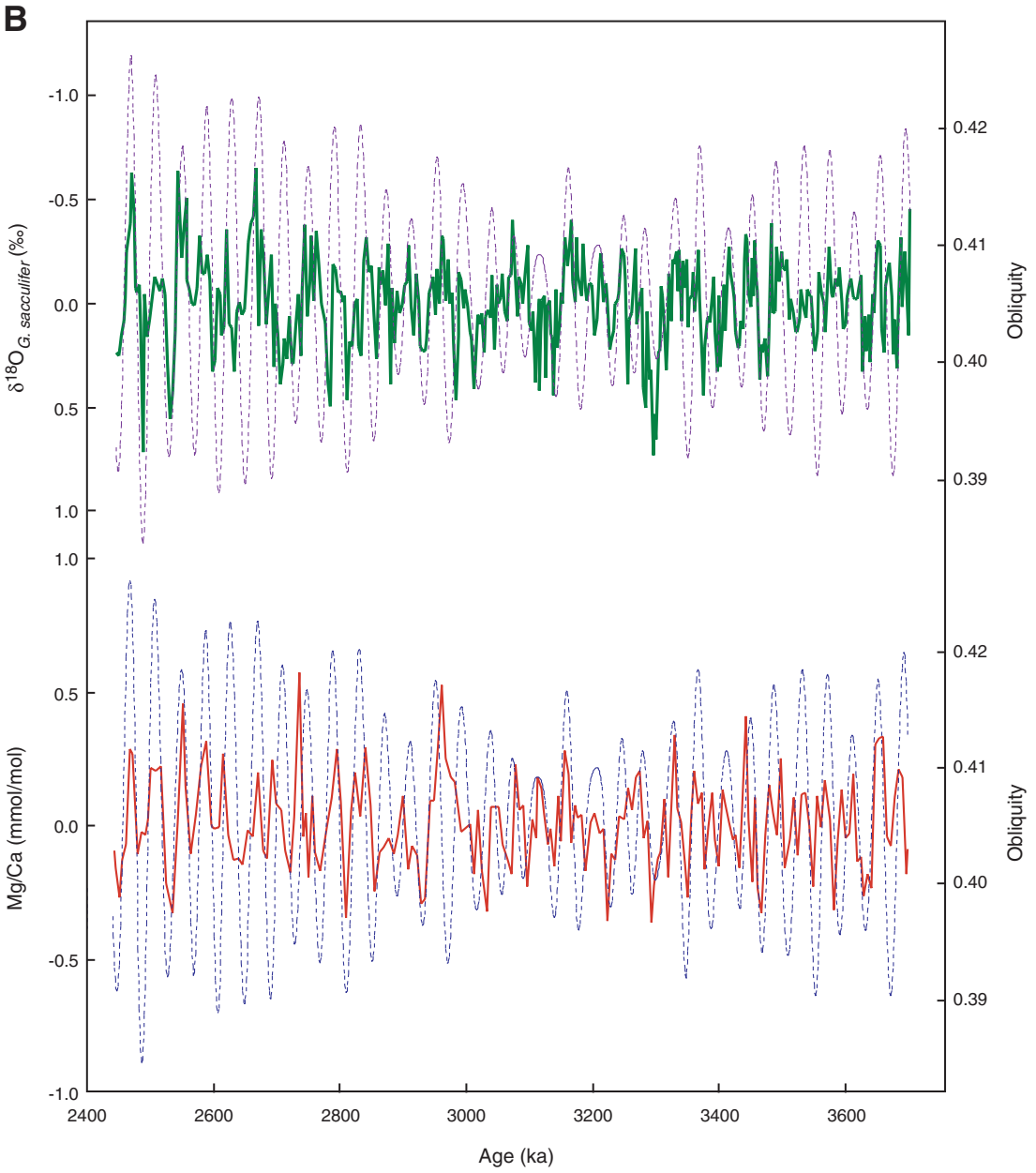

Figure F4. Spectral analysis for the time interval 3.7–2.4 Ma. Time series analyses were performed with AnalySeries 1.2 (Paillard et al., 1996). **A.** $\delta^{18}O$, measured on benthic foraminifers (**Tiedemann et al.,** this volume). **B.** Mg/Ca ratios, measured in foraminiferal tests of the planktonic foraminifer *Globigerinoides sacculifer.* **C.** $\delta^{18}O$, measured in foraminiferal tests of the planktonic foraminifer *G. sacculifer.* **D.** $\delta^{18}O_{salinity}$, calculated by subtracting the normalized $\delta^{18}O_{benthic}$ record from the $\delta^{18}O_{water}$ record.

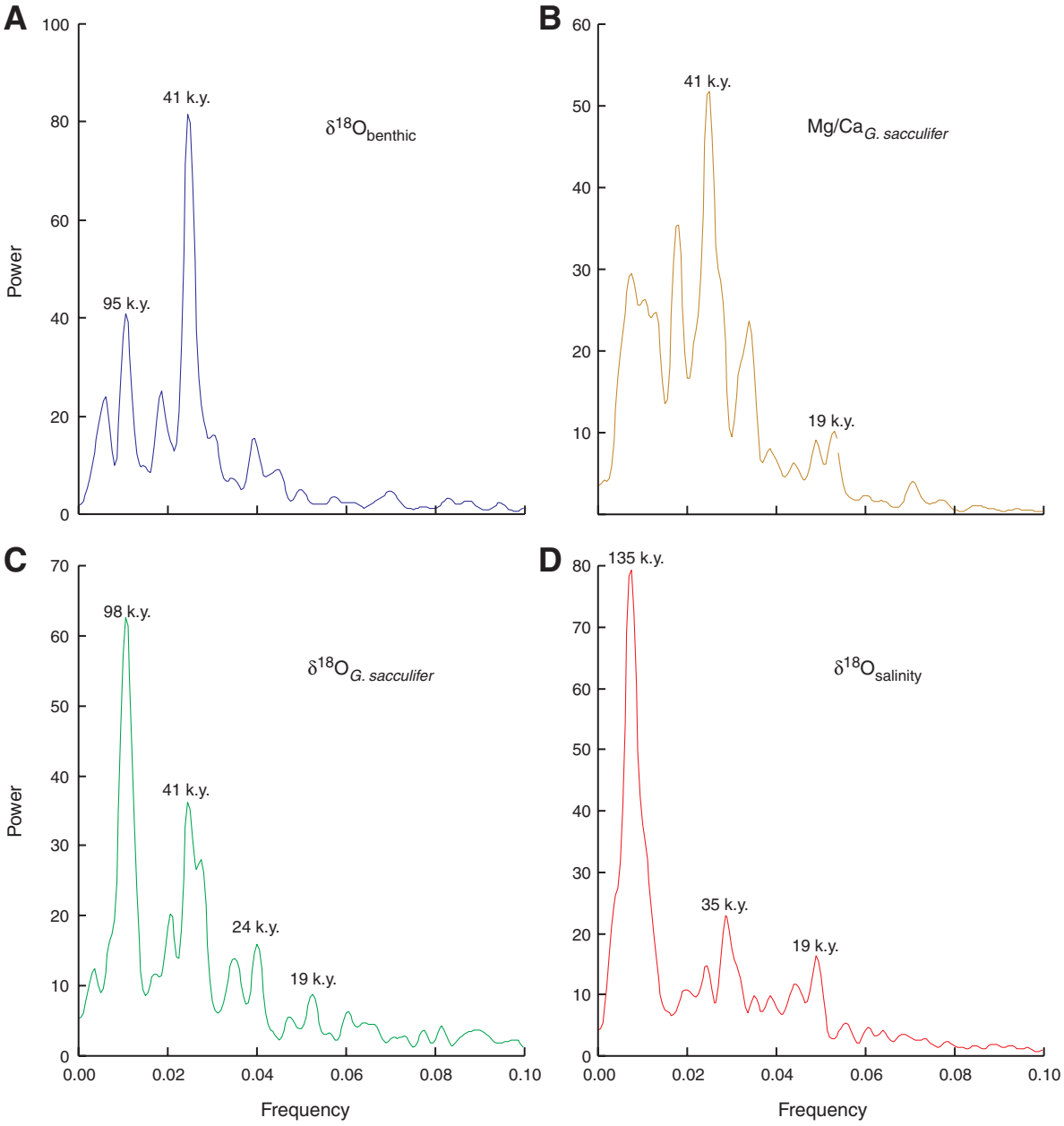

Figure F5. Spectral analysis for the time interval 4.8–3.7 Ma. Time series analyses were performed with AnalySeries 1.2 (Paillard et al., 1996). **A.** $\delta^{18}O$, measured on benthic foraminifers (**Tiedemann et al.,** this volume). **B.** Mg/Ca ratios, measured in foraminiferal tests of the planktonic foraminifer *Globigerinoides sacculifer.* **C.** $\delta^{18}O$, measured in foraminiferal tests of the planktonic foraminifer *G. sacculifer.* **D.** $\delta^{18}O_{salinity}$, calculated by subtracting the normalized $\delta^{18}O_{benthic}$ record from the $\delta^{18}O_{water}$ record.

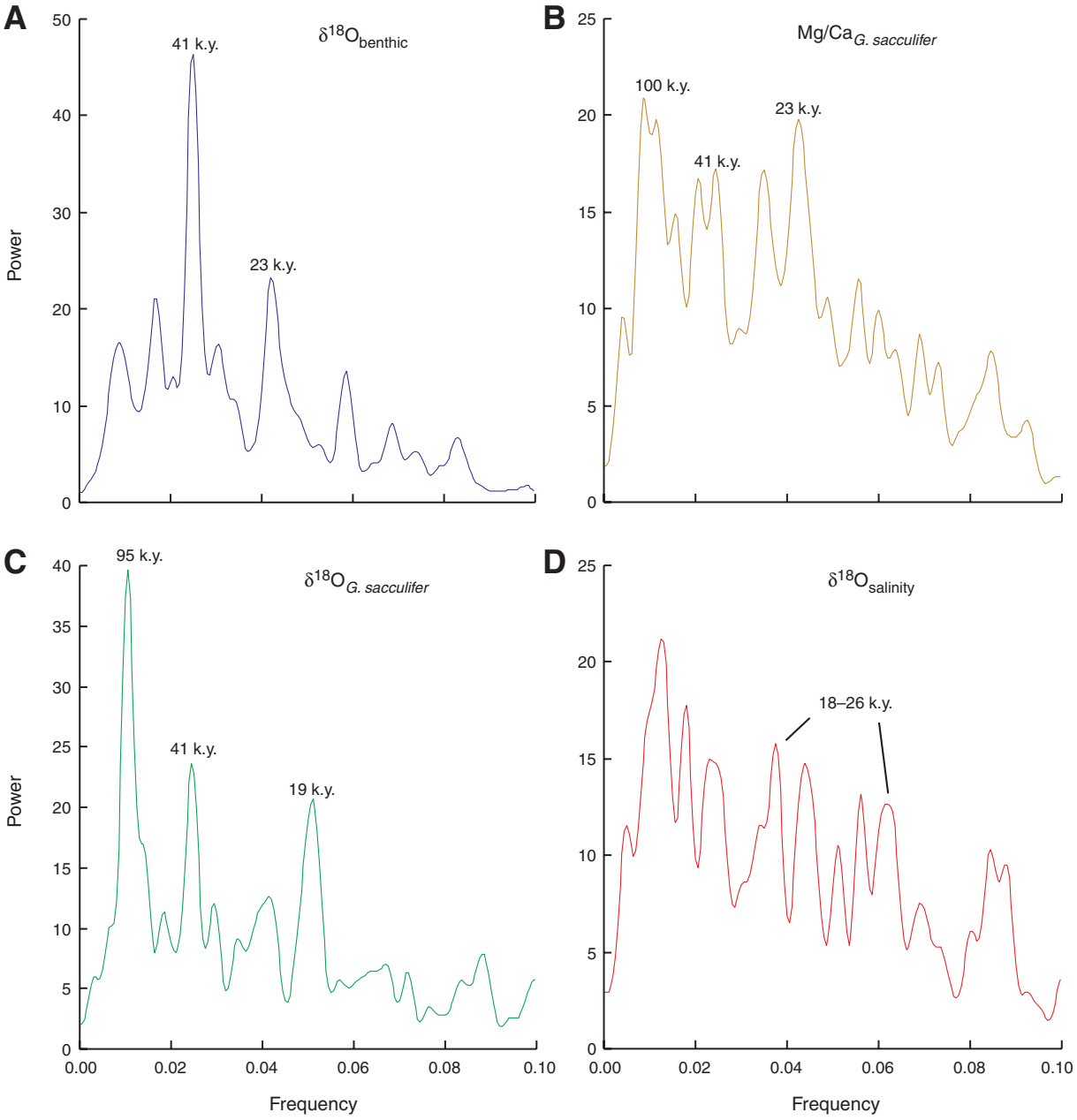

Figure F6. Comparison between tropical east and west Pacific sea-surface temperatures (SSTs) for the time interval 4.2–2.4 Ma. East Pacific SSTs are Mg/Ca SSTs from Site 1241. West Pacific SSTs are results from planktonic foraminiferal transfer functions, Modern Analog Technique (MAT), from Andersson (1997) for Ontong Java Plateau Site 806 (0°19′N, 159°21′E). * = modern SST values at the paleolocation of Site 1241.

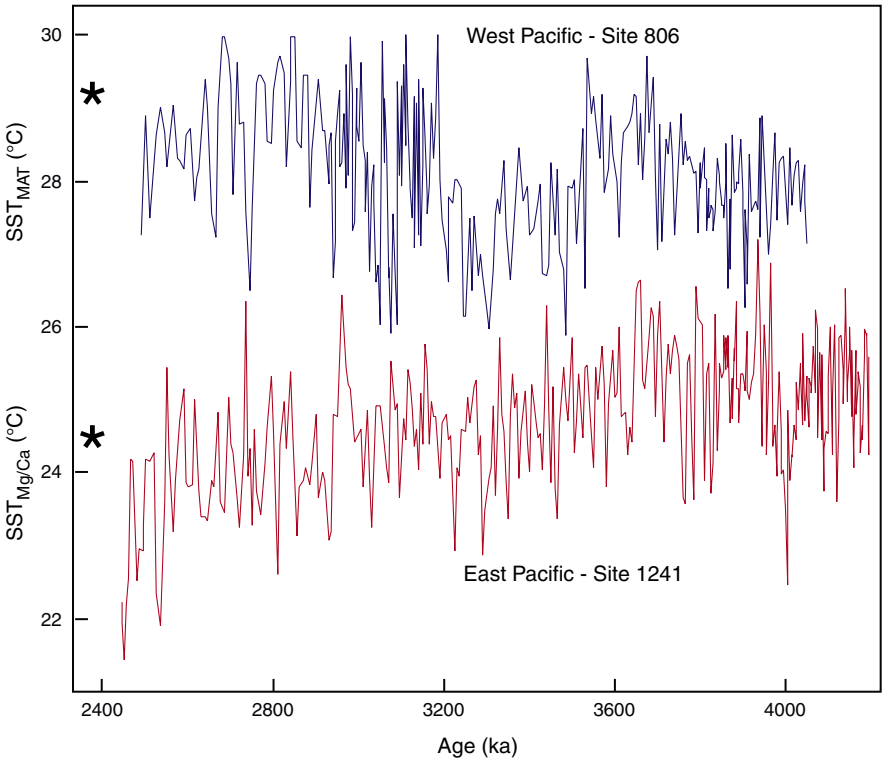

Table T1. Cross spectral analysis for Mg/Ca and $\delta^{18}O_{G.sacculifer}$, Site 1241.

Target	Reference	Time interval (Ma)	Frequency	Cyclicity (k.y.)	Coherency	Phase	Lag (k.y.)
Mg/Ca	Insolation 65°N*	3.7–2.4	0.024	41	0.90	–0.03	–0.2
$\delta^{18}O_{G.sacculifer}$	Insolation 65°N*	3.7–2.4	0.025	41	0.96	–0.20	–1.3
$\delta^{18}O_{benthic}$†	Insolation 65°N*	3.7–2.4	0.024	41	0.95	0.13	0.8
Mg/Ca	$\delta^{18}O_{benthic} \times -1$†	3.7–2.4	0.024	41	0.91	–0.19	–1.3
Mg/Ca	$\delta^{18}O_{G.sacculifer} \times -1$	3.7–2.4	0.024	41	0.92	0.09	0.6
Mg/Ca	Insolation 65°N*	4.8–3.7	0.052	19	0.87	0.88	2.7
Mg/Ca	Insolation 65°N*	4.8–3.7	0.044	23	0.88	0.46	1.7
$\delta^{18}O_{G.sacculifer}$	Insolation 65°N*	4.8–3.7	0.024	41	0.81	1.20	7.8
Mg/Ca	$\delta^{18}O_{G.sacculifer} \times -1$	4.8–3.7	0.053	19	0.80	0.23	0.7
Mg/Ca	$\delta^{18}O_{G.sacculifer} \times -1$	4.8–3.7	0.042	23	0.87	–0.08	–0.3

Notes: * = Laskar (1990). † = **Tiedemann et al.,** this volume.